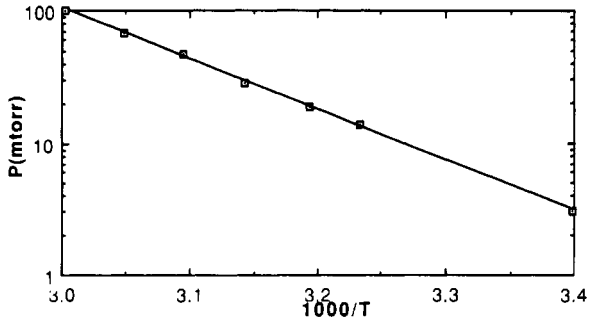

Figure 6. Plot of log (vapor pressure, P) versus $1/T$ for (hfac)Cu(PMe_3).

repeated sublimation and freeze–pump–thaw cycles. Above 60 °C, the change in measured pressure with time was large and may result from thermal instability of this compound perhaps via the dissociation of PMe_3. The enthalpy of vaporization, ΔH_{vap}, of (hfac)Cu(PMe_3) was calculated to be approximately 10 kcal/mol from the plot of log (vapor pressure) versus $1/T$ shown in Figure 6. This value is comparable to that observed for Cu(hfac)$_2$.[10]

Attempts to measure the vapor pressures of (acac)Cu(PMe_3) and (tfac)Cu(PMe_3) were unsuccessful due to the inability to obtain constant vapor pressures at a given temperature. This may be due to the poor thermal stability of those species over extended time periods.

Acknowledgment. We thank the NSF and Motorola for support of this work. M.J.H.-S. thanks the NSF Chemical Instrumentation program for the purchase of a low-field NMR spectrometer. T.T.K. acknowledges support from an NSF Presidential Young Investigator Award (CTS9058538).

Supplementary Material Available: For (hfac)Cu(PMe_3), Tables S1–S3 (structure determination summary), Tables S4 and S5 (bond lengths and angles), Tables S6 and S7 (anisotropic displacement coefficients, H atom coordinates, and isotropic displacement coefficients), Figures S1–S3 (atom-numbering schemes for molecules 1–3) and Figure S4 (unit cell diagram), for (dpm)Cu(PMe_3), Tables S8–S10 (structure determination summary), Tables S11 and S12 (bond lengths and angles), Tables S13 and S14 (anisotropic displacement coefficients, H atom coordinates, and isotropic displacement coefficients), Figure S5 (atom-numbering scheme for molecule 2), and Figure S6 (unit cell diagram), and for (dbm)Cu(PMe_3), Tables S15–S17 (structure determination summary), Tables S18 and S19 (bond lengths and angles), Tables S20 and S21 (anisotropic displacement coefficients, H atom coordinates, and isotropic displacement coefficients), and Figure S7 (unit cell diagram), for naphthalene, Cu(hfac)$_2$, and (hfac)Cu(PMe_3), Figures S8–S10 (vapor pressure vs time), and textual presentations of the experimental procedure for the (hfa)Cu(PMe_3) vapor pressure measurement and spectroscopic characterization data for (tfac)Cu(PMe_3), (acac)Cu(PMe_3), (dpm)Cu(PMe_3), (dbm)Cu(PMe_3), (tfac)Cu(PMe_3)$_2$, and (acac)Cu(PMe_3)$_2$ (43 pages); Tables S22–S24 (observed and calculated structure factors for (hfac)Cu(PMe_3), (dpm)Cu(PMe_3), and (dbm)Cu(PMe_3)) (39 pages). Ordering information is given on any current masthead page.

Contribution from the Department of Chemistry and Center for Fundamental Materials Research, Michigan State University, East Lansing, Michigan 48824

Hydrothermal Polychalcogenide Chemistry. Stabilization of $[Mo_9Se_{40}]^{8-}$, a Cluster of Clusters, and $[Mo_3Se_{18}]_n^{2n-}$, a Polymeric Polyselenide. Novel Phases Based on Trinuclear $[Mo_3Se_7]^{4+}$ Building Blocks

Ju-Hsiou Liao and Mercouri G. Kanatzidis*

Received May 15, 1991

A polymeric Mo polyselenide, $K_2Mo_3Se_{18}$, and a large molecular cluster Mo polyselenide, $K_8Mo_9Se_{40}\cdot 4H_2O$, were synthesized by the hydrothermal method. The reaction of Mo, K_2Se_4, and H_2O in a 1:1.5:22.2 ratio in a vacuum-sealed Pyrex tube at 135 °C for 3 days yielded black platelike crystals of $K_2Mo_3Se_{18}$ (I). The reaction of MoO_3, K_2Se_2, and H_2O in a 1:2:22.2 ratio under the same conditions as above yielded black chunky crystals of $K_8Mo_9Se_{40}\cdot 4H_2O$ (II). Both compounds were obtained in ~20% yield. The structures were determined by single-crystal X-ray diffraction techniques. Crystal data for $K_2Mo_3Se_{18}$: monoclinic $P2_1$, $Z = 2$, $a = 10.277$ (6) Å, $b = 12.66$ (1) Å, $c = 10.624$ (8) Å, $\beta = 116.82$ (5)°, $V = 1233$ (2) Å^3; $2\theta_{max}$(Mo Kα) = 45°; number of data measured 1824, number of unique data 1608, number of data having $F_o^2 > 3\sigma(F_o^2)$ 1382, number of variables 207, number of atoms 23; $\mu = 267$ cm^{-1}; final $R = 0.052$ and $R_w = 0.086$. Crystal data for $K_8Mo_9Se_{40}\cdot 4H_2O$: triclinic $P\bar{1}$, $Z = 2$, $a = 10.312$ (8) Å, $b = 18.55$ (3) Å, $c = 18.57$ (2) Å, $\alpha = 87.6$ (1)°, $\beta = 87.57$ (7)°, $\gamma = 84.0$ (1)°, $V = 3523$ (8) Å^3; $2\theta_{max}$(Mo Kα) = 45°; number of data measured 9888, number of unique data 8638, number of data having $F_o^2 > 4\sigma(F_o^2)$ 3592, number of variables 546, number of atoms 65; $\mu = 224$ cm^{-1}; final $R = 0.092$ and $R_w = 0.108$. I and II have rather complicated structures. I contains the $[Mo_3(Se)(Se_2)_3(Se_3)(Se_4)_2]_n^{2n-}$ polymeric anion which contains $[Mo_3Se_7]^{4+}$ clusters as building blocks. It has a zigzag chain structure which is formed by two parallel sets of face-to-face $[Mo_3Se_7]^{4+}$ clusters cross-linked by Se_4^{2-} ligands. The zigzag chains are then arranged side by side and interact through weak Se···Se contacts generated by a Se atom of a Se_3^{2-} ligand of one chain and the triangular face of Se atoms from the three bridging Se_2^{2-} ligands of a $[Mo_3Se_7]^{4+}$ cluster in another chain. $[Mo_9Se_{40}]^{8-}$ contains three trinuclear $[Mo_3Se_7]^{4+}$ subclusters which are "glued" together by the two monoselenide ions. One monoselenide ion belongs to a $[Mo_3Se_7]^{4+}$ core being coordinated to three Mo atoms and at the same time interacting with the triangular face of three Se atoms of Se_2^{2-} bridging ligands of another $[Mo_3Se_7]^{4+}$ subcluster. The other monoselenide ion interacts with six Se atoms of Se_2^{2-} bridging ligands of two $[Mo_3Se_7]^{4+}$ subclusters. Two separate $[Mo_9Se_{40}]^{8-}$ clusters come in close contact (2.98 Å) in the solid state through two terminal Se_2^{2-} ligands related by an inversion center.

Introduction

Metal polychalcogenides are of longstanding interest in the field of coordination and solid-state chemistry.[1] Conventionally, syntheses of molecular metal polychalcogenides are carried out in solution at ambient temperature.[2,3] Recently, molten salts have

(1) (a) Ansari, M. A.; Ibers, J. A. *Coord. Chem. Rev.* **1990**, *100*, 223–266. (b) Kolis, J. W. *Coord. Chem. Rev.* **1990**, *105*, 195–219. (c) Draganjac, M.; Rauchfuss, T. B. *Angew. Chem., Int. Ed. Engl.* **1985**, *24*, 742–757. (d) Müller, A. *Polyhedron* **1986**, *5*, 323–340. (e) Kanatzidis, M. G. *Comments Inorg. Chem.* **1990**, *10*, 161–195.

(2) (a) Flomer, W. A.; O'Neal, S. C.; Cordes, A. W.; Jetter, D.; Kolis, J. W. *Inorg. Chem.* **1988**, *27*, 969–971. (b) Wardle, R. W. M.; Mahler, C. H.; Chau, C.-N.; Ibers, J. A. *Inorg. Chem.* **1988**, *27*, 2790–2795. (c) Adel, J.; Weller, F.; Dehnicke, K. *Z. Naturforsch.* **1988**, *43B*, 1094–1100. (d) Eichhorn, B. W.; Haushalter, R. C.; Cotton, F. A.; Wilson, B. *Inorg. Chem.* **1988**, *27*, 4085–4095. (e) Strasdeit, H.; Krebs, B.; Henkel, G. *Inorg. Chim. Acta* **1984**, *89*, L11–L13.

0020-1669/92/1331-0431$03.00/0

been used to synthesize new solid-state metal polychalcogenides.[4,5] Our interest in exploring unusual conditions for the stabilization and crystallization of new metal–chalcogenide frameworks led us to consider hydrothermal techniques as a possible alternative. Despite the invaluable contributions of hydrothermal techniques in important areas such as zeolite synthesis,[6] quartz[7] and potassium titanyl phosphate (KTP)[8] crystal growth, and synthesis of other interesting oxides,[9] the application of hydrothermal methods to prepare ternary metal chalcogenides is very rare in the literature, except with some notable examples.[10] Hydrothermal conditions with metal sulfides have been examined in the past primarily by geologists to study the formation of sulfide minerals. Recently, hydrothermal and methanothermal conditions using CO_3^{2-} and OH^- as mineralizers were used to digest sulfides and selenides of main-group metals to yield new phases such as $Cs_4Sn_5S_{12}\cdot 2H_2O$,[10a] $RbSb_3Se_5$,[10b] $Rb_2Sb_4S_7$,[10c] $KAsSe_3\cdot H_2O$,[10d] $RbAsSe_3\cdot 0.5H_2O$,[10d] $CsAsSe_3\cdot 0.5H_2O$,[10d] $Cs_4Sn_2Se_6$,[10e] and $K_4Sn_3Se_8$.[10f] Furthermore, Bedard et al. recently reported that novel germanium–sulfide network structures could be synthesized by hydrothermal methods similar to those used for zeolites.[11] Most of these compounds contain monochalcogenide ligands. We felt that if polychalcogenide ligands were used instead, as mineralizers as well as reagents, *polychalcogenide* phases may be accessible. As part of our recent investigations, in this technique, we used various Se_x^{2-} ligands in combination with metals or metal oxides as starting materials to synthesize new ternary metal polyselenides. In a previous communication, we reported the hydrothermal synthesis of a large Mo polychalcogenide cluster, $K_{12}Mo_{12}Se_{56}$,[12] with unexpected and unprecedented structural features. We report here our further investigations into the hydrothermal chemistry of the K/Mo/Se system which revealed two more new Mo polyselenides: $K_2Mo_3Se_{18}$ (I) and $K_8Mo_9Se_{40}\cdot 4H_2O$ (II), exhibiting not only novel structures but also features not found in $K_{12}Mo_{12}Se_{56}$.

Experimental Section

All work was done under a nitrogen atmosphere. Mo and MoO_3 were purchased from Alfa Products Inc. Potassium polyselenide K_2Se_x (x = 2, 4) was prepared in liquid ammonia from potassium metal and elemental selenium in a 2:x ratio. The X-ray powder diffraction patterns were recorded with a Phillips XRG-3000 computer controlled powder diffractometer operating at 40 kV/20 mA. Ni-filtered Cu radiation was used. Elemental analyses were performed on a JEOL JSM-35C scanning electron microscope (SEM) equipped with an energy dispersive spectroscopy (EDS) detector.

Synthesis of $[K_2Mo_3Se_{18}]_n$ (I). A mixture of 0.048 g (0.5 mmol) of Mo metal, 0.296 g (0.75 mmol) of K_2Se_4, and 0.2 mL of H_2O was placed in a Pyrex tube, which was vacuum-sealed and heated at 135 °C for 3 days. Black platelike crystals of $K_2Mo_3Se_{18}$ (I) formed, and they were isolated by filtration and washed with methanol. Yield: ~20%.

Synthesis of $K_8Mo_9Se_{40}\cdot 4H_2O$ (II). The reaction of 0.072 g (0.5 mmol) of MoO_3, 0.236 g (1.0 mmol) of K_2Se_2, and 0.2 mL of H_2O under the same conditions as above yielded black chunky crystals of $K_8Mo_9Se_{40}\cdot 4H_2O$ (II). The products were isolated by filtration and washed with methanol. The compound was obtained in ~20% yield.

In order to ensure product homogeneity, the X-ray powder diffraction (XRD) diagrams of both products were compared with, and found to be identical with, those calculated from the single-crystal data. The XRD powder patterns were calculated using the atom coordinates determined from the single-crystal data with the program POWD 10.[13] Comparison tables between the calculated and observed d_{hkl} spacings for these com-

Table I. Data for the Crystal Structure Analysis[a] of $K_2Mo_3Se_{18}$ and $K_8Mo_9Se_{48}\cdot 4H_2O$

formula	$K_2Mo_3Se_{18}$	$K_8Mo_9Se_{48}\cdot 4H_2O$
fw	1724.3	4398.7
a, Å	10.277 (6)	10.312 (8)
b, Å	12.66 (1)	18.55 (3)
c, Å	10.624 (8)	18.57 (2)
α, deg	90.0	87.6 (1)
β, deg	116.82 (5)	87.57 (7)
γ, deg	90.00	84.0 (1)
V, Å^3; Z	1233; 2	3523; 2
space group	$P2_1$	$P\bar{1}$
D_{calcd}, g/cm^3	4.64	4.08
μ(Mo Kα), cm^{-1}	267	224
2θ range, deg	4–45	4–45
no. of data collected	1824	9888
no. of unique data	1608	8638
no. of data used	1382 ($F_o^2 > 3\sigma(F_o^2)$)	3592 ($F_o^2 > 4\sigma(F_o^2)$)
min/max abs cor	0.40/0.99	0.71/0.99
no. of variables	207	546
no. of atoms per asym unit	23	65
final R/R_w,[b] %	5.2/8.6	9.2/10.8

[a] At −120 °C. [b] $R = \Sigma(|F_o| - |F_c|)/\Sigma|F_o|$; $R_w = [\Sigma w(|F_o| - |F_c|)^2/\Sigma w|F_o|^2]^{1/2}$.

Table II. Fractional Atomic Coordinates and B_{eq} Values for $K_2Mo_3Se_{18}$[a]

atom	x	y	z	B_{eq}, Å^2
Mo1	0.9101 (5)	0.2306 (4)	0.5096 (5)	0.6 (1)
Mo2	0.7514 (5)	0.239	0.6609 (5)	0.7 (1)
Mo3	1.0540 (5)	0.2517 (4)	0.8013 (5)	0.6 (1)
Se1	0.8955 (6)	0.3909 (6)	0.6358 (6)	1.3 (1)
Se2	0.9100 (7)	0.1551 (6)	0.2759 (7)	1.7 (2)
Se3	0.8919 (7)	0.3381 (6)	0.2923 (6)	1.3 (1)
Se4	0.8894 (7)	0.9054 (6)	0.6891 (7)	2.0 (2)
Se5	1.1006 (6)	0.1014 (6)	0.6678 (6)	1.2 (1)
Se6	1.1909 (6)	0.2642 (6)	0.6409 (7)	1.5 (1)
Se7	0.8928 (7)	0.2820 (6)	0.9308 (6)	1.3 (1)
Se8	0.9077 (6)	0.1111 (5)	0.8543 (6)	1.1 (1)
Se9	0.7363 (6)	0.0857 (5)	0.4960 (6)	1.1 (1)
Se10	0.6269 (6)	0.2450 (6)	0.3854 (6)	1.1 (1)
Se11	1.1740 (7)	0.4348 (6)	0.9024 (7)	1.8 (2)
Se12	1.4217 (7)	0.4282 (6)	1.0738 (6)	1.5 (1)
Se13	0.5642 (7)	−0.0363 (6)	0.7027 (7)	1.5 (1)
Se14	0.5263 (6)	0.1495 (5)	0.6714 (6)	1.1 (1)
Se15	1.2831 (7)	0.1891 (6)	1.0340 (7)	1.4 (1)
Se16	1.2375 (8)	0.0043 (6)	1.0190 (8)	2.2 (2)
Se17	0.5389 (6)	0.4265 (6)	0.8310 (6)	1.3 (1)
Se18	0.5544 (6)	0.3871 (6)	0.6217 (6)	1.5 (1)
K1	0.736 (2)	0.652 (2)	0.661 (2)	3.2 (4)
K2	0.585 (2)	0.190 (2)	1.007 (2)	3.7 (5)

[a] Estimated standard deviations are given in parentheses.

(3) (a) Kanatzidis, M. G.; Huang, S.-P. *Angew. Chem., Int. Ed. Engl.* **1989**, *28*, 1513–1514. (b) Kanatzidis, M. G.; Dhingra, S. *Inorg. Chem.* **1989**, *28*, 2024–2026. (c) Huang, S.-P.; Dhingra, S.; Kanatzidis, M. G. *Polyhedron* **1990**, *9*, 1389–1395. (d) Kanatzidis, M. G.; Huang, S.-P. *J. Am. Chem. Soc.* **1989**, *111*, 760–761.

(4) (a) Kanatzidis, M. G. *Chem. Mater.* **1990**, *2*, 353–363. (b) Kanatzidis, M. G.; Park, Y. *J. Am. Chem. Soc.* **1989**, *111*, 3767–3769. (c) Park, Y.; Kanatzidis, M. G. *Angew. Chem., Int. Ed. Engl.* **1990**, *29*, 914–915. (d) Kanatzidis, M. G.; Park, Y. *Chem. Mater.* **1990**, *2*, 99–101.

(5) Sunshine, S. A.; Kang, D.; Ibers, J. A. *J. Am. Chem. Soc.* **1987**, *109*, 6202–6204. (b) Kang, D.; Ibers, J. A. *Inorg. Chem.* **1988**, *27*, 549–551.

(6) Barrer, R. M. *Hydrothermal Chemistry of Zeolites*; Academic Press: New York, 1982.

(7) Laudise, R. A. *Chem. Eng. News* **1987**, *65* (Sept 28), 30–43.

(8) Stucky, G. D.; Phillips, M. L. F.; Gier, T. E. *Chem. Mater.* **1989**, *1*, 492–509.

(9) (a) Huan, G.; Jacobson, J. W.; Corcoran, E. W. *Chem. Mater.* **1990**, *2*, 91–93. (b) Corcoran, E. W. *Inorg. Chem.* **1990**, *29*, 158–160. (c) Mundi, L. A.; Strohmaier, K. G.; Goshom, D. P.; Haushalter, R. C. *J. Am. Chem. Soc.* **1990**, *112*, 8182–8183. (d) Haushalter, R. C. *Inorg. Chem.* **1989**, *28*, 2904–2905.

(10) (a) Sheldrick, W. S. *Z. Anorg. Allg. Chem.* **1988**, *562*, 23–30. (b) Sheldrick, W. S.; Hauser, H.-J. *Z. Anorg. Allg. Chem.* **1988**, *557*, 98–104. (c) Sheldrick, W. S.; Hauser, H.-J. *Z. Anorg. Allg. Chem.* **1988**, *557*, 105–111. (d) Sheldrick, W. S.; Kaub, J. *Z. Anorg. Allg. Chem.* **1986**, *535*, 179–185. (e) Sheldrick, W. S.; Braunbeck, H. G. *Z. Naturforsch.* **1989**, *44B*, 851–852. (f) Sheldrick, W. S. *Z. Naturforsch.* **1988**, *43B*, 249–252. (g) Parise, J. B. *Science* **1991**, *251*, 293–294. (h) Parise, J. B. *J. Chem. Soc., Chem. Commun.* **1990**, 1553–1554.

(11) Bedard, R. L.; Wilson, S. T.; Vail, L. D.; Bennett, E. M.; Flanigen, E. M. *Zeolites; Facts, Figures, Future*; Jacobs, P. A., van Santen, R. A., Eds.; Elsevier: New York, 1989; pp 375–387.

(12) Liao, J.-H.; Kanatzidis, M. G. *J. Am. Chem. Soc.* **1990**, *112*, 7400–7402.

(13) Smith, D. K.; Nichols, M. C.; Zolensky, M. E. POWD 10: A FORTRAN Program for Calculating X-ray Powder Diffraction Patterns (Version 10). Pennsylvania State University, 1983.

pounds are deposited in the supplementary material.

X-ray Crystallographic Studies. The crystallographic data were collected on a Nicolet P3/F diffractometer using an $\omega/2\theta$ scan mode and Mo Kα radiation. The crystals were mounted on the tip of glass fibers. Crystal data and details for data collection and refinement for both compounds are shown in Table I. The intensities of three check reflections were monitored every 100 reflections to detect possible decay during the data collection period. An empirical absorption correction was applied to all data on the basis of ψ scans for several reflections. An additional absorption correction following the DIFABS[14] procedure was applied to isotropically refined data. All structures were refined by full-matrix least-squares techniques with the SDP[15] package of crystallographic programs running on a VAXstation 2000 computer.

Solution of the Structure of $[K_2Mo_3Se_{18}]_n$. Although crystals of I also diffract weakly, there was no observed decay. The data were collected using a 2°/min scan speed at −120 °C. The structure was solved with direct methods using SHELXS-86[16] and was refined normally. No disorder was found in the unit cell of I. All atoms were refined anisotropically. The final R and R_w values were 5.2% and 8.6%, respectively. The enantiomorph was also refined to completion but gave slightly higher R values (~0.5%) and estimated standard deviations (esd's). There were no significant residual peaks in the final electron density difference map. The final coordinates and thermal parameters and their esd's of all atoms are shown in Table II.

Solution of the Structure of $K_8Mo_9Se_{40}\cdot 4H_2O$. Crystals of II diffracted weakly. Initially, data were collected at room temperature, using Cu radiation from a rotating-anode source for a crystal which decayed by ~50% (based on the intensities of three standard reflections) during the data collection period. The scan speed was 6°/min. The structure of the anion was solved using this data with SHELXS-86 and was refined down to R = 14%. At this point, it was evident from electron difference density maps that some of the K atoms were disordered in the unit cell and that water molecules might be present. Only five of the eight K atoms could be located with confidence. The poor quality of the data did not permit the resolution of the positions of the remaining atoms and prompted us to recollect another data set from a another crystal at −120 °C using sealed-tube Mo radiation. The scan speed was 2°/min. No decay was detected in this second set of data. Although these new data were significantly better, still they were not superb and only ~40% of the reflections were observed. The structure was solved again ab initio, and the same Mo/Se framework was found. Electron difference density maps calculated from this improved data set revealed the positions of four ordered K atoms and four disordered K atoms. On the basis of refinement of the temperature factors of the disordered K atoms, their occupancy was deemed to be 0.50. Four oxygen atoms belonging to water molecules were also located. At this point it is reasonable to suggest that the likely cause of the decay in crystallinity of the first crystal was due to loss of solvated water. No disorder was found in the anion. The Mo, Se, and K atoms were refined anisotropically, while the oxygen atoms were refined isotropically. The final R and R_w values were 9.2% and 10.8%, respectively. There were no significant residual peaks in the final electron density difference map. The final coordinates and thermal parameters and their esd's of all atoms are shown in Table III.

Results and Discussion

Synthesis. The syntheses of $K_2Mo_3Se_{18}$ and $K_8Mo_9Se_{40}\cdot 4H_2O$ were performed in thick-wall Pyrex glass tubes at 130–140 °C. Although a very small amount of water was used (12% filling), at no time during the reaction was it completely evaporated and the crystals grew in the liquid phase of the container. The small volume of water used is beneficial because it generates supersaturation conditions and promotes crystal growth. Crystals of $K_2Mo_3Se_{18}$ rarely grow larger than 0.5 mm. However, crystals of $K_8Mo_9Se_{40}\cdot 4H_2O$ have been obtained as large as ~5 mm on an edge. The amount of reagents and water used is important to ensure phase reproducibility. We have found that minor variations in synthetic conditions lead to other phases which currently are under investigation.[17] I is insoluble in water and most organic solvents, while II is soluble in water, dimethylformamide, and dimethyl sulfoxide. On the basis of their structures (vide infra) and the fact that I and II are diamagnetic, the Mo formal oxidation state can be assigned as +4. The for-

Table III. Fractional Atomic Coordinates and B_{eq} Values for the $K_8Mo_9Se_{40}\cdot 4H_2O$[a]

atom	x	y	z	B_{eq}, Å^2
Mo1	0.1803 (6)	0.9003 (5)	0.6476 (3)	3.9 (2)
Mo2	−0.0490 (5)	0.8866 (4)	0.7266 (3)	2.9 (2)
Mo3	−0.0189 (5)	0.8364 (5)	0.5891 (3)	3.5 (2)
Mo4	0.3960 (6)	0.6065 (4)	0.7706 (3)	2.6 (2)
Mo5	0.1642 (5)	0.5922 (4)	0.8506 (3)	2.2 (1)
Mo6	0.2030 (6)	0.5328 (5)	0.7159 (4)	3.9 (2)
Mo7	0.4907 (5)	1.1616 (4)	0.9112 (4)	3.0 (2)
Mo8	0.5137 (6)	1.1808 (4)	0.7625 (4)	3.4 (2)
Mo9	0.2701 (6)	1.1849 (4)	0.8295 (4)	3.7 (2)
Se1	−0.0321 (7)	0.9677 (6)	0.6152 (5)	5.0 (2)
Se2	0.4325 (7)	0.9059 (6)	0.6513 (4)	4.9 (2)
Se3	0.3065 (8)	1.0096 (6)	0.6130 (5)	7.7 (3)
Se4	−0.2191 (8)	0.9774 (5)	0.7875 (5)	5.1 (2)
Se5	−0.1576 (7)	0.8691 (5)	0.8532 (4)	3.5 (2)
Se6	−0.0761 (7)	0.7380 (7)	0.5025 (4)	5.6 (3)
Se7	−0.1505 (7)	0.8596 (6)	0.4743 (4)	6.1
Se8	0.1712 (6)	0.8317 (5)	0.7708 (3)	2.2 (2)
Se9	0.1370 (7)	0.9560 (5)	0.7735 (5)	4.7 (2)
Se10	−0.0767 (6)	0.7550 (5)	0.6984 (3)	2.2 (2)
Se11	−0.2432 (6)	0.8414 (5)	0.6611 (3)	3.1 (2)
Se12	0.1893 (7)	0.8655 (7)	0.5123 (4)	6.5 (3)
Se13	0.2109 (6)	0.7731 (6)	0.5994 (3)	4.0 (2)
Se14	0.1809 (6)	0.6665 (5)	0.7371 (3)	2.9 (2)
Se15	0.6473 (7)	0.6193 (6)	0.7652 (4)	4.4 (2)
Se16	0.5091 (7)	0.7205 (5)	0.7260 (4)	3.8 (2)
Se17	−0.0092 (6)	0.6902 (5)	0.9013 (3)	2.7 (2)
Se18	0.0403 (7)	0.5857 (6)	0.9778 (4)	3.8 (2)
Se19	0.0764 (8)	0.5489 (7)	0.5990 (4)	6.7 (3)
Se20	0.152 (1)	0.4308 (6)	0.6312 (5)	8.6 (3)
Se21	0.3896 (7)	0.5449 (5)	0.8963 (4)	3.6 (2)
Se22	0.3396 (7)	0.6722 (5)	0.8912 (3)	2.6 (2)
Se23	0.1574 (7)	0.4574 (5)	0.8306 (5)	4.1 (2)
Se24	−0.0206 (6)	0.5374 (5)	0.7888 (4)	3.1 (2)
Se25	0.4327 (7)	0.4731 (6)	0.7361 (5)	5.2 (2)
Se26	0.4078 (7)	0.5663 (6)	0.6399 (4)	5.8 (2)
Se27	0.4284 (7)	1.0723 (5)	0.8250 (4)	2.8 (2)
Se28	0.5779 (7)	1.0630 (5)	1.0027 (4)	4.2 (2)
Se29	0.5972 (7)	1.1821 (5)	1.0349 (4)	4.5 (2)
Se30	0.6352 (7)	1.1007 (6)	0.6644 (4)	4.1 (2)
Se31	0.6466 (8)	1.2269 (6)	0.6498 (5)	5.3 (2)
Se32	0.0675 (7)	1.1164 (6)	0.8226 (5)	4.9 (2)
Se33	0.0277 (8)	1.2433 (7)	0.8226 (8)	9.4 (4)
Se34	0.6112 (7)	1.2610 (5)	0.8488 (5)	4.1 (2)
Se35	0.7164 (6)	1.1434 (5)	0.8400 (4)	3.2 (2)
Se36	0.3034 (7)	1.1832 (6)	0.6900 (5)	5.2 (2)
Se37	0.3430 (7)	1.2875 (6)	0.7498 (6)	5.4 (2)
Se38	0.3142 (7)	1.2678 (6)	0.9286 (6)	5.4 (3)
Se39	0.2575 (7)	1.1514 (6)	0.9676 (5)	4.9 (2)
Se40	0.4239 (8)	0.3935 (6)	0.8667 (7)	6.9 (3)
K1	0.474 (2)	0.137 (2)	0.5158 (9)	7.8 (8)
K2	0.516 (2)	0.893 (1)	0.817 (1)	5.2 (5)
K3	0.053 (2)	0.847 (2)	0.332 (1)	9.2 (9)
K4	0.329 (2)	0.293 (1)	0.101 (1)	6.4 (6)
K5	0.090 (2)	0.821 (2)	0.002 (2)	6 (1)
K5′	0.097 (3)	−1.026 (2)	0.050 (2)	4.5 (9)
K6	0.270 (3)	0.565 (2)	0.110 (1)	6 (1)
K6′	0.137 (1)	0.718 (3)	0.048 (2)	2.9 (8)*
K7	−0.233 (4)	0.506 (3)	0.639 (2)	4 (1)*
K7′	0.260 (3)	0.431 (3)	0.051 (2)	7 (1)
K8	−0.527 (4)	1.375 (3)	0.547 (2)	7 (1)
K8′	0.345 (5)	0.521 (3)	0.474 (3)	9 (1)*
O1	0.238 (6)	0.621 (5)	0.453 (4)	10 (2)*
O2	0.086 (6)	0.668 (5)	0.353 (3)	9 (2)*
O3	0.398 (5)	0.281 (4)	0.455 (3)	6 (1)*
O4	0.195 (4)	0.613 (3)	0.253 (2)	5 (1)*

[a] Estimated standard deviations are given in parentheses. Starred values indicate atoms were refined anisotropically. Anisotropically refined atoms are given in the form of the isotropic equivalent displacement parameter defined as follows: $(4/3)[a^2B(1,1) + b^2B(2,2) + c^2B(3,3) + ab(\cos\gamma)B(1,2) + ac(\cos\beta)B(1,3) + bc(\cos\alpha)B(2,3)]$.

(14) Walker, N.; Stuart, D. DIFABS: An Empirical Method for Correcting Diffractometer Data for Absorption Effects. *Acta Crystallogr.* **1983**, *A39*, 158–166.
(15) Frenz, B. A. The Enraf-Nonius CAD4 SDP System. *Computing in Crystallography*; Delft University Press: Delft, Holland, 1978; pp 64–71.
(16) Sheldrick, G. M. In *Crystallographic Computing 3*; Sheldrick, G. M., Kruger, C., Goddard, R., Eds.; Oxford University Press: Oxford, U.K., 1985; pp 175–189.
(17) Liao, J.-H.; Hill, L.; Kanatzidis, M. G. Work in progress.

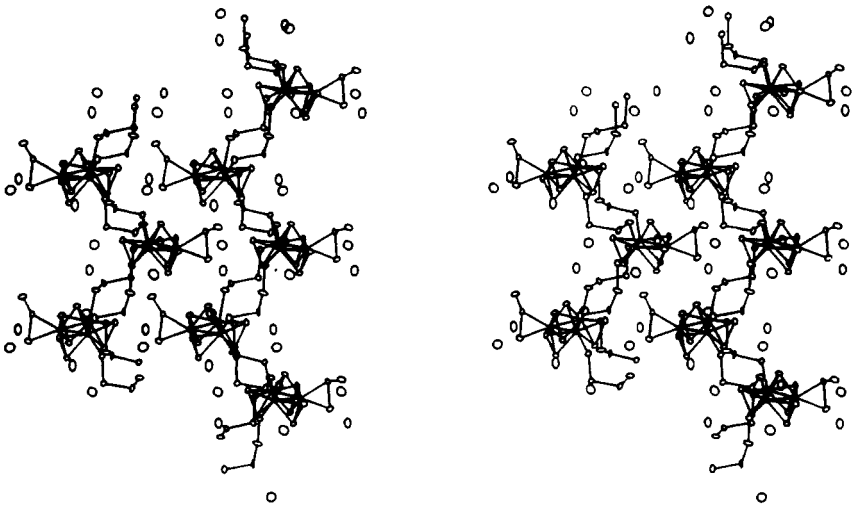

Figure 1. ORTEP representation of a stereoview of two "interlocking" zigzag chains of $[Mo_3Se_{18}]_n^{2n-}$. The isolated open circles are K atoms.

mation of I and II involves complicated redox reactions between Mo, MoO_3, and K_2Se_x. In the case of $K_2Mo_3Se_{18}$, molybdenum metal is oxidized by the Se–Se bonds in Se_4^{2-}, while in the case of $K_8Mo_9Se_{40}\cdot 4H_2O$, Mo^{6+} in MoO_3 is reduced by Se_2^{2-}. Use of longer polyselenides such as Se_4^{2-}, Se_5^{2-}, and Se_6^{2-}, to reduce MoO_3, was found unsuitable because oxidation to elemental selenium was favored.

It is interesting to comment on how these K/Mo/Se phases might form. The fact that the $[Mo_3Se_7]^{4+}$ core occurs in all three phases characterized thus far suggests that the core has considerable thermodynamic stability and forms readily under hydrothermal conditions. In solution, the trinuclear $[Mo_3Se_7]^{4+}$ core is probably ligated by Se_x^{2-} ligands. The various $\{[Mo_3Se_7](Se_x)_n\}^{2-}$ complexes present in solution during the reaction provide an efficient mass-transport and dissolution–reprecipitation mechanism, both of which are necessary for crystal growth. Thus the excess Se_x^{2-} ligands act as effective "mineralizers". The role of counterion in phase formation is not clear at the moment, but preliminary observations indicate that it must be significant. For example, new structure types have been isolated when Cs instead of K is used.[17] We presume the fate of the oxide ion to be hydroxide, after reaction with water. Since the selenide ion is softer than oxide, the substitution of the latter, in MoO_3, by Se_x^{2-} is assisted by the reduction of the Mo^{6+} center to the softer Mo^{4+} center.

We note here that known Mo/Se anions such as $[MoSe_4]^{2-}$[18] and $[MoSe_9]^{2-}$,[19] typically synthesized at ambient temperature using conventional solution methods, were not observed under our hydrothermal conditions nor did we observe $MoSe_2$ impurities. We also did not detect formation of reduced Mo/Se Chevrel phases, such as the members of the $A_{n-2}[Mo_{3n}Se_{3n+2}]$ (A = alkali-metal ion) family,[20] typically prepared by high temperature ceramic methods.

Structure Description. The Polymeric $[Mo_3Se_{18}]_n^{2n-}$. $[Mo_3Se_{18}]_n^{2n-}$ is the first known molybdenum polyselenide polymer. The structure of $[Mo_3Se_{18}]_n^{2n-}$ is illustrated in Figure 1. It is composed of a zigzag-chain-like structure containing the repeating unit shown in Figure 2. It is also worthwhile to point out that the compound contains four different polyselenides (Se^{2-}, Se_2^{2-}, Se_3^{2-}, and Se_4^{2-}) as ligands, even though only Se_4^{2-} was used as starting material. The starting tetraselenide is reduced by Mo metal to form shorter selenides, while Mo metal is oxidized to the formal oxidation state of 4+. The presence of all the different

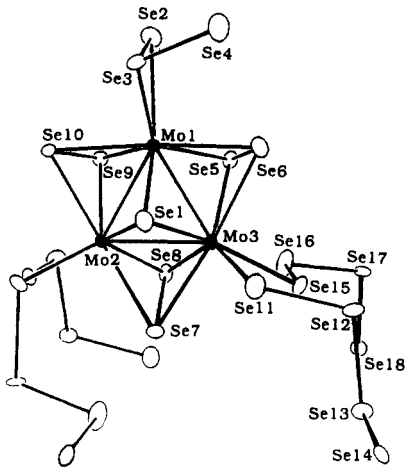

Figure 2. Labeling scheme of the repeating unit of $[Mo_3Se_{18}]_n^{2n-}$.

polyselenides also attests to the complexity of polyselenide solutions.[1e]

The anion framework contains the discrete trinuclear $[Mo_3(\mu_2\text{-}Se_2)_3(\mu_3\text{-}Se)]^{4+}$ cluster core as a building block. The clusters are connected in space by one Se_3^{2-} and two Se_4^{2-} ligands. The average Mo–Mo distance in the core is 2.77 (1) Å, and it is comparable to that of the similar building block found in $[Mo_{12}Se_{56}]^{12-}$[12] and in the molybdenum polysulfide cluster $[Mo_3S_{13}]^{2-}$.[21] The latter contains the $[Mo(\mu_2\text{-}S_2)_3(\mu_3\text{-}S)]^{4+}$ core, which is also found as a repeating unit in the polymeric structure of $Mo_3S_7X_4$ (X = Cl, Br).[22] An interesting feature of this core is that the three Mo atoms and three Se atoms from the $\mu_2\text{-}Se_2^{2-}$ ligands lie in the same plane. The remaining three Se atoms from the $\mu_2\text{-}Se_2^{2-}$ ligands lie above this plane opposite to the $\mu_3\text{-}Se^{2-}$ ligand. Recently, Soviet workers reported the interesting sulfo/seleno complex $[Mo_2S_4Se_3Cl_6]^{2-}$ containing a similar trinuclear $[Mo(\mu\text{-}SSe)_3(\mu_3\text{-}S)]^{4+}$ core.[23]

The zigzag chain of $[Mo_3(\mu_2\text{-}Se_2)_3(\mu_3\text{-}Se)(Se_4)_2(Se_3)]_n^{2n-}$ can be viewed as parallel $[Mo_3(\mu_2\text{-}Se_2)_3(\mu_3\text{-}Se)]^{4+}$ cores, facing in the same direction and cross-linked by bridging Se_4^{2-} ligands. The latter bond to the two Mo atoms (Mo2 and Mo3) of the $[Mo_3(\mu_2\text{-}Se_2)_3(\mu_3\text{-}Se)]^{4+}$ cores. The zigzag chains are noncentrosym-

(18) Müller, A.; Diemann, E.; Jostes, R.; Bögge, H. *Angew. Chem., Int. Ed. Engl.* **1981**, *20*, 934–955.
(19) O'Neal, S. C.; Kolis, J. W. *J. Am. Chem. Soc.* **1988**, *110*, 1971–1973.
(20) (a) Potel, M.; Gougeon, P.; Chevrel, R.; Sergent, M. *Rev. Chim. Miner.* **1984**, *21*, 509–536. (b) Chevrel, R.; Sergent, M. In *Superconductivity in Ternary Compounds*; Fisher, O., Maple, M. P., Eds.; Topics in Current Physics; Springer-Verlag: Berlin, 1982. (c) Gougeon, P.; Potel, M.; Sergent, M. *Acta Crystallogr.* **1989**, *C45*, 182–185.
(21) (a) Müller, A.; Pohl, S.; Dartmann, M.; Cohen, J. P.; Bennett, J. M.; Kirshner, R. M. *Z. Naturforsch.* **1979**, *34B*, 434–436. (b) Müller, A.; Sarkar, S.; Bhattacharyya, R. G.; Pohl, S.; Dartmann, M. *Angew. Chem., Int. Ed. Engl.* **1978**, *17*, 535.
(22) Marcoll, J.; Rabenau, A.; Mootz, D.; Wunderlich, H. *Rev. Chim. Miner.* **1974**, *11*, 607–615.
(23) Fedin, V. P.; Mironov, Yu. V.; Sokolov, M. N.; Kolesov, B. A.; Fedorov, V. Ye.; Yufit, D. S.; Struchkov, Yu. T. *Inorg. Chim. Acta* **1990**, *174*, 275–282.

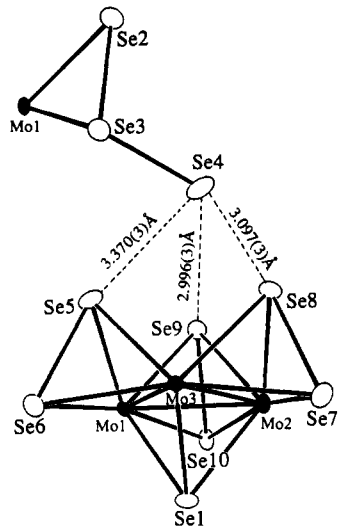

Figure 3. ORTEP representation of the interaction between the Se_3^{2-} ligand and the $[Mo_3(\mu_3\text{-}Se)(\mu_2\text{-}Se_2)_3]^{4+}$ core in $[Mo_3Se_{18}]_n^{2n-}$.

Table IV. Selected Distances (Å) in the $[Mo_3Se_{18}]_n^{2n-}$ Chain

Mo1–Mo2	2.759 (2)	Mo3–Se5	2.544 (3)
Mo1–Mo3	2.779 (2)	Mo3–Se6	2.660 (3)
Mo2–Mo3	2.781 (2)	Mo3–Se7	2.615 (3)
Mo1–Se1	2.473 (3)	Mo3–Se8	2.551 (3)
Mo1–Se2	2.660 (3)	Mo3–Se11	2.617 (3)
Mo1–Se3	2.613 (3)	Mo3–Se15	2.651 (2)
Mo1–Se5	2.522 (3)	Se3–Se4	2.327 (3)
Mo1–Se6	2.612 (3)	Se4–Se8	3.097 (3)
Mo1–Se9	2.519 (3)	Se5–Se6	2.330 (3)
Mo1–Se10	2.604 (2)	Se2–Se3	2.336 (3)
Mo2–Se1	2.513 (3)	Se4–Se9	2.996 (3)
Mo2–Se7	2.621 (3)	Se9–Se10	2.350 (3)
Mo2–Se8	2.539 (3)	Se7–Se8	2.340 (3)
Mo2–Se9	2.572 (3)	Se13–Se14	2.382 (3)
Mo2–Se10	2.613 (2)	Se15–Se16	2.376 (3)
Mo2–Se14	2.625 (3)	Se17–Se18	2.354 (3)
Mo2–Se18	2.650 (3)	Se11–Se12	2.370 (3)
Mo3–Se1	2.503 (3)	Se16–Se17	2.342 (3)
		Se12–Se13	2.356 (3)

[a] Standard deviations are given in parentheses.

metric. All the triply bridging Se atoms in the $[Mo_3(\mu_2\text{-}Se_2)_3(\mu_3\text{-}Se)]^{4+}$ units within a single zigzag chain are pointed to the (010) direction. The third Mo atom, Mo3, is bonded to a terminal Se_3^{2-} ligand in an unusual fashion. In this triselenide ligand, two adjacent Se atoms, Se2 and Se3, are bonded to Mo3, while the third terminal Se4 atom is left alone. This is shown in Figure 3. What is unprecedented is that Se4 stretches out to the center of a triangle of three Se atoms of the three bridging diselenides of another $[Mo_3(\mu_2\text{-}Se_2)_3(\mu_3\text{-}Se)]^{4+}$ cluster in a neighboring chain. This generates an unusual polyselenide fragment similar, but not identical, to the $[Se_7]^{8-}$ "umbrella" found in $[Mo_{12}Se_{56}]^{12-}$. This fragment is shown in Figure 3 and in structure **1**. The bond

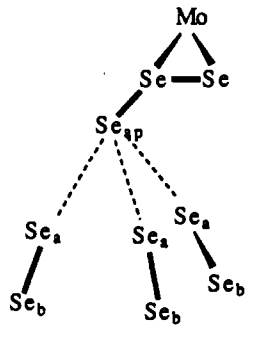

1

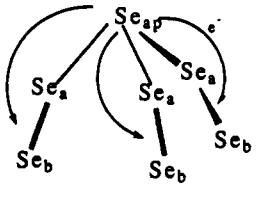

2

distances in the triselenide unit are 2.336 (3) and 2.327 (3) Å,

Table V. Selected Angles (deg) in the $[Mo_3Se_{18}]^{2-}$ Chain[a]

Mo2–Mo1–Mo3	60.27 (6)	Se2–Mo1–Se3	52.58 (7)
Se1–Mo1–Se2	145.7 (1)	Se2–Mo1–Se5	93.57 (8)
Se1–Mo1–Se3	93.11 (9)	Se2–Mo1–Se6	95.28 (9)
Se1–Mo1–Se5	112.93 (9)	Se2–Mo1–Se9	89.03 (8)
Se1–Mo1–Se6	84.23 (8)	Se2–Mo1–Se10	91.28 (8)
Se1–Mo1–Se9	114.45 (9)	Se3–Mo1–Se5	130.6 (1)
Se1–Mo1–Se10	83.70 (8)	Se3–Mo1–Se6	90.48 (8)
Se8–Mo2–Se9	83.75 (8)	Se3–Mo1–Se9	124.21 (9)
Se8–Mo2–Se10	137.4 (1)	Se3–Mo1–Se10	84.13 (8)
Se8–Mo2–Se14	86.41 (8)	Se5–Mo1–Se6	53.94 (8)
Se8–Mo2–Se18	137.51 (9)	Se5–Mo1–Se9	83.30 (8)
Se9–Mo2–Se10	53.89 (8)	Se5–Mo1–Se10	137.50 (9)
Se9–Mo2–Se14	85.35 (8)	Se6–Mo1–Se9	137.17 (9)
Se9–Mo2–Se18	128.29 (9)	Se6–Mo1–Se10	166.5 (1)
Se10–Mo2–Se14	93.70 (8)	Se9–Mo1–Se10	54.57 (8)
Se10–Mo2–Se18	81.40 (8)	Se7–Mo2–Se8	53.90 (7)
Se14–Mo2–Se18	71.72 (8)	Se7–Mo2–Se9	137.28 (9)
Se1–Mo2–Se7	83.99 (8)	Se7–Mo2–Se10	165.8 (1)
Se1–Mo2–Se8	112.72 (9)	Se7–Mo2–Se14	96.14 (9)
Se1–Mo2–Se9	111.28 (9)	Se7–Mo2–Se18	91.86 (8)
Se1–Mo2–Se10	82.74 (8)	Se1–Mo2–Se18	83.55 (8)
Se1–Mo2–Se14	155.3 (1)		
Se1–Mo3–Se5	111.18 (9)	Se6–Mo3–Se7	166.43 (9)
Se1–Mo3–Se6	82.66 (8)	Se6–Me3–Se8	135.89 (9)
Se1–Mo3–Se7	84.30 (8)	Se6–Mo3–Se11	85.55 (8)
Se1–Mo3–Se8	112.64 (9)	Se6–Mo3–Se15	96.38 (8)
Se1–Mo3–Se11	72.64 (8)	Se7–Mo3–Se8	53.85 (7)
Se1–Mo3–Se15	152.6 (1)	Se7–Mo3–Se11	87.00 (8)
Se5–Mo3–Se6	53.14 (8)	Se7–Mo3–Se15	93.47 (8)
Se5–Mo3–Se7	136.58 (9)	Se8–Mo3–Se11	138.0 (1)
Se5–Mo3–Se8	83.09 (8)	Se8–Mo3–Se15	87.12 (8)
Se5–Mo3–Se11	135.90 (9)	Se11–Mo3–Se15	79.99 (8)
Se5–Mo3–Se15	89.12 (8)		
Mo1–Se1–Mo2	67.20 (7)	Mo2–Se9–Se4	104.91 (8)
Mo1–Se1–Mo3	67.90 (7)	Mo2–Se8–Se7	64.82 (8)
Mo1–Se5–Mo3	66.53 (7)	Mo2–Se9–Se10	63.95 (8)
Mo1–Se6–Mo3	63.63 (7)	Mo1–Se6–Se5	61.08 (8)
Mo1–Se9–Mo2	65.65 (7)	Mo2–Se7–Se8	61.28 (8)
Mo1–Se10–Mo2	63.87 (6)	Mo2–Se14–Se13	109.9 (1)
Mo2–Se1–Mo3	67.33 (7)	Mo3–Se6–Se5	60.89 (8)
Mo2–Se7–Mo3	64.16 (7)	Mo3–Se7–Se8	61.69 (8)
Mo2–Se8–Mo3	66.22 (7)	Mo3–Se15–Se16	99.6 (1)
Mo1–Se3–Se2	64.74 (9)	Mo2–Se18–Se17	112.0 (1)
Mo1–Se3–Se4	115.7 (1)	Mo1–Se5–Se6	64.99 (8)
Mo1–Se2–Se3	62.67 (8)	Mo3–Se5–Se6	65.98 (8)
Mo3–Se8–Se7	64.47 (8)	Mo1–Se10–Se9	60.87 (8)
Mo1–Se9–Se4	112.05 (9)	Mo2–Se10–Se9	62.16 (8)
Mo1–Se9–Se10	64.55 (8)	Mo3–Se11–Se12	115.4 (1)
Se2–Se3–Se4	105.3 (1)	Se15–Se16–Se17	105.4 (1)
Se3–Se4–Se9	121.8 (1)	Se16–Se17–Se18	105.6 (1)
Se11–Se12–Se13	108.9 (1)	Se4–Se9–Se10	168.9 (1)
Se12–Se13–Se14	105.1 (1)		

[a] Standard deviations are given in parentheses.

respectively, which are in the range of other normal Se–Se distances.[1,2] The average distance between Se_{ap} and Se_a is 3.15 (16) Å (see **1**). The distance between two parallel $[Mo_3(\mu_2\text{-}Se_2)_3(\mu_3\text{-}Se)]^{4+}$ triangles in each individual chain is 12.66 Å, which allows for the insertion of another such triangle from the neighboring chain. This brings the zigzag chains together side by side in a staggered arrangement to make two-dimensional sheets. The single chains interlock in a "zipper fashion". The average distance between these sheets is 9.17 Å, with the potassium atoms located between. Selected distances and angles in the Mo/Se framework are shown in Tables IV and V. There are two crystallographically different potassium atoms with coordination numbers of 9 and 10, respectively, shown in Figure 4. The average K–Se distance is 3.6 (2) Å. Selected K–Se distances are given in Table VIII.

The average Se–Se distances in the tetraselenide ligands are normal at 2.36 (2) Å. The three bridging diselenides in the $[Mo_3(\mu_2\text{-}Se_2)_3(\mu_3\text{-}Se)]^{4+}$ core have the average bond distance of 2.34 (1) Å, which is 0.11 Å shorter than what is observed in the same $[Mo_3(\mu_2\text{-}Se_2)_3(\mu_3\text{-}Se)]^{4+}$ cores of $K_{12}Mo_{12}Se_{56}$. Structure **2** shows the $[Se_7]^{8-}$ "umbrella" fragment found in $[Mo_{12}Se_{56}]^{12-}$.

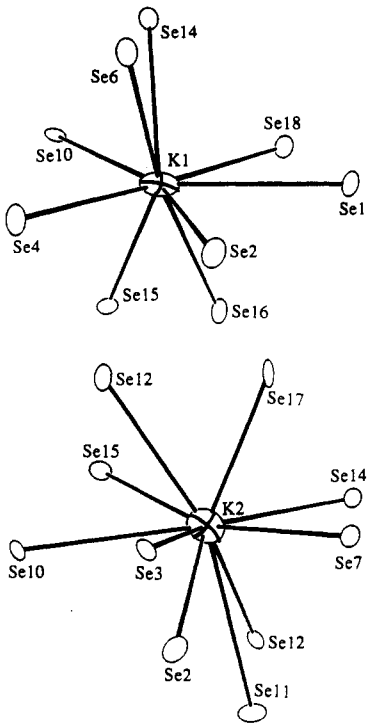

Figure 4. ORTEP representation of the environments of K1 and K2 in $[K_2Mo_3Se_{18}]_n$.

The average Se_{ap}–Se_b distance in $[Mo_{12}Se_{56}]^{12-}$ is 2.76 (15) Å. The interaction of Se_{ap} (formally a Se^{2-} unit) with the bridging diselenides could be the result of partial electron transfer from the Se_{ap} to the Se_a–Se_b unit. This is suggested by the significant lengthening of the average Se_a–Se_b distance (2.45 (7) Å) in $[Mo_{12}Se_{56}]^{12-}$, as noted previously.[12] Structure **I** shows the formation of a similar "umbrella" polyselenide fragment found in I. However, in this case, the apical Se_{ap} atom is actually a terminal Se atom of a triselenide ligand bound to a $[Mo_3(\mu_2\text{-}Se_2)_3(\mu_3\text{-}Se)]^{4+}$ cluster. The Se_{ap}–Se_a distances in I are longer (average 3.15 (16) Å) than those found in $[Mo_{12}Se_{56}]^{12-}$ but significantly shorter than 4.0 Å, the sum of van der Waals radii of two Se atoms.[24] If indeed electron transfer were responsible for such short contacts in I, it is not extensive enough to lengthen the Se_a–Se_b diselenide bonds in I. This could arise from the higher formal oxidation state of Se_{ap} (1–) in I compared to that (2–) in $[Mo_{12}Se_{56}]^{12-}$. Theoretical calculations are in progress to probe the influence of the apical selenium on the corresponding diselenides in the $[Mo_3(Se_2)_3Se]^{4+}$ core.

The $[Mo_9Se_{40}]^{8-}$ Cluster of Clusters. The $[Mo_9Se_{40}]^{8-}$ anion has a very unusual and asymmetric structure, which is shown in Figure 5. It has several unexpected features. It is composed of three different trinuclear molybdenum polyselenide subclusters, A–C, in which the trinuclear $[Mo_3(\mu_2\text{-}Se_2)_3(\mu_3\text{-}Se)]^{4+}$ core is readily recognizable. The $[Mo_9Se_{40}]^{8-}$ anion can be viewed as an aggregate of three $[Mo_3Se_{13}]^{2-}$ trinuclear clusters and one Se^{2-}. The average Mo–Mo distance in A–C is 2.77 (1) Å, similar to that in $[Mo_3Se_{18}]_n^{2n-}$, $[Mo_{12}Se_{56}]^{12-}$,[12] and $[Mo_3Se_{13}]^{2-}$.[21] The triply bridging Se14 atom is part of subcluster B by covalently binding its three Mo atoms and at the same time forming unusual Se···Se contacts with the three Se atoms of the bridging Se^{2-} units of subcluster A. The average bond distance is 3.13 (6) Å, which is significantly smaller than the van der Waals distance between two Se atoms. This Se···Se interaction is probably not bonding and does not cause significant bond lengthening of the bridging diselenides in cluster A. We note that the approach of two $[Mo_3(\mu_2\text{-}Se_2)_3(\mu_3\text{-}Se)]^{4+}$ cores in this fashion is also unprecedented. The average Se–Se distance in the bridging Se_2^{2-} ligands in subcluster A is 2.31 (2) Å. Selected distances and angles in the Mo/Se framework are shown in Tables VI and VII. The coordination around the K^+ ions is not well defined in terms of regular coordination polyhedra, but it ranges from 8 to 11. The distances around the K^+ ions are given in Table VIII.

Table VI. Selected Distances (Å) in the $[Mo_9Se_{40}]^{8-}$ Anion[a]

Mo–Mo Distances					
Mo1–Mo2	2.760 (6)	Mo4–Mo5	2.791 (5)	Mo7–Mo8	2.773 (6)
Mo1–Mo3	2.759 (5)	Mo4–Mo6	2.778 (5)	Mo7–Mo9	2.775 (5)
Mo2–Mo3	2.749 (6)	Mo5–Mo6	2.772 (6)	Mo8–Mo9	2.750 (6)
		Mo–Mo (mean)	2.77 (1)		
Mo–Se Distances					
Mo1–Se1	2.489 (7)	Mo6–Se24	2.620 (6)	Mo7–Se27	2.499 (6)
Mo1–Se8	2.574 (6)	Mo4–Se15	2.624 (6)	Mo7–Se28	2.562 (8)
Mo1–Se2	2.617 (6)	Mo6–Se25	2.543 (8)	Mo7–Se29	2.646 (6)
Mo1–Se3	2.568 (8)	Mo4–Se14	2.467 (6)	Mo7–Se34	2.543 (7)
Mo3–Se12	2.618 (6)	Mo6–Se26	2.606 (6)	Mo7–Se35	2.625 (6)
Mo1–Se9	2.599 (8)	Mo4–Se16	2.609 (7)	Mo7–Se38	2.559 (7)
Mo1–Se12	2.615 (7)	Mo4–Se21	2.558 (6)	Mo7–Se39	2.604 (6)
Mo1–Se13	2.542 (9)	Mo4–Se25	2.567 (8)	Mo8–Se27	2.503 (7)
Mo2–Se1	2.517 (7)	Mo4–Se26	2.563 (6)	Mo8–Se30	2.594 (7)
Mo2–Se4	2.560 (8)	Mo5–Se14	2.481 (6)	Mo8–Se31	2.616 (7)
Mo2–Se5	2.584 (6)	Mo5–Se17	2.589 (6)	Mo8–Se34	2.536 (7)
Mo2–Se8	2.544 (5)	Mo6–Se19	2.571 (7)	Mo8–Se35	2.606 (6)
Mo4–Se22	2.608 (6)	Mo6–Se20	2.617 (7)	Mo8–Se36	2.596 (5)
Mo3–Se11	2.617 (6)	Mo5–Se18	2.641 (6)	Mo8–Se37	2.517 (7)
Mo2–Se9	2.616 (6)	Mo5–Se21	2.563 (6)	Mo9–Se27	2.514 (7)
Mo2–Se10	2.565 (7)	Mo5–Se22	2.611 (6)	Mo9–Se32	2.567 (6)
Mo2–Se11	2.615 (5)	Mo5–Se23	2.552 (8)	Mo9–Se33	2.624 (7)
Mo3–Se1	2.491 (9)	Mo5–Se24	2.584 (6)	Mo9–Se36	2.599 (7)
Mo3–Se6	2.609 (8)	Mo6–Se14	2.513 (8)	Mo9–Se37	2.520 (8)
Mo3–Se7	2.572 (5)	Mo6–Se23	2.553 (8)	Mo9–Se38	2.531 (8)
Mo3–Se10	2.567 (6)			Mo9–Se39	2.615 (7)
Mo3–Se13	2.543 (7)				
Se–Se Distances					
Se2–Se3	2.32 (1)	Se25–Se26	2.44 (1)	Se21–Se40	2.866 (9)
Se4–Se5	2.350 (9)	Se28–Se28	2.98 (1)	Se23–Se40	2.969 (7)
Se6–Se7	2.35 (1)	Se28–Se29	2.342 (8)	Se25–Se40	2.80 (1)
Se8–Se9	2.297 (8)	Se30–Se31	2.360 (9)	Se34–Se40	2.984 (8)
Se10–Se11	2.329 (7)	Se32–Se33	2.35 (1)	Se37–Se40	3.182 (9)
Se12–Se13	2.307 (8)	Se34–Se35	2.340 (8)	Se38–Se40	2.87 (1)
Se15–Se16	2.344 (9)	Se36–Se37	2.349 (9)		
Se17–Se18	2.380 (8)	Se38–Se39	2.37 (1)		
Se19–Se20	2.31 (1)				
Se21–Se22	2.362 (8)				
Se23–Se24	2.373 (8)				

[a] Standard deviations are given in parentheses. The estimated standard deviation in the mean Mo–Mo bond length was calculated from the equation $\sigma_l = [\sum_n (l_n - l)^2/n(n-1)]^{1/2}$, where l_n is the length of the nth bond, l the mean length, and n the number of bonds.

Another unprecedented interaction is that between subcluster B and subcluster C. These subclusters are connected by a Se^{2-} ion which is weakly interacting with six Se atoms of the six Mo-bridging Se_2^{2-} units of the two subclusters. This forms an intriguing $[Se_{13}]^{x-}$ "double-umbrella" fragment, shown in structure **3**, with long Se_{ap}–Se_a distances, as shown in Figure 5. The distance

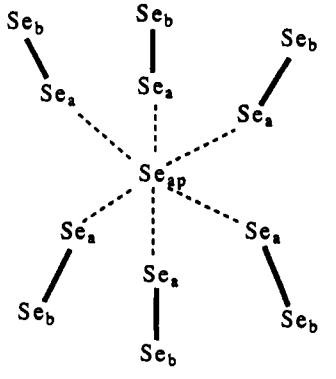

3

between this Se_{ap} atom and the six Se atoms ranges from 2.80

(24) Weast, R. C. *CRC Handbook of Chemistry and Physics*; CRC Press: Boca Raton, FL, 1985–1988; Vol. 66, p D-188.

Table VII. Selected Bond Angles (deg) for $[Mo_9Se_{40}]^{8-}$ [a]

				Subcluster A			
Se2–Mo1–Se3	53.0 (2)	Se1–Mo2–Se4	92.4 (3)	Mo1–Se1–Mo2	66.9 (2)	Mo1–Se9–Mo2	63.9 (2)
Se2–Mo1–Se8	92.6 (2)	Se1–Mo2–Se9	85.1 (2)	Mo1–Se1–Mo3	67.3 (2)	Mo1–Se9–Se8	63.2 (2)
Se2–Mo1–Se9	92.9 (2)	Se1–Mo2–Se10	113.0 (2)	Mo2–Se1–Mo3	66.6 (2)	Mo2–Se9–Se8	62.0 (2)
Se2–Mo1–Se12	93.9 (2)	Se1–Mo2–Se11	83.5 (2)	Mo1–Se2–Se3	62.4 (2)	Mo2–Se10–Mo3	64.8 (2)
Se2–Mo1–Se13	92.1 (2)	Se4–Mo2–Se5	54.4 (2)	Mo1–Se3–Se2	64.7 (2)	Mo2–Se10–Se11	64.4 (2)
Se3–Mo1–Se9	86.9 (3)	Se4–Mo2–Se11	86.6 (2)	Mo2–Se4–Se5	63.3 (2)	Mo2–Se11–Mo3	63.4 (2)
Se3–Mo1–Se12	89.8 (3)	Se5–Mo2–Se9	94.0 (2)	Me2–Se5–Se4	62.3 (2)	Mo2–Se11–Se10	62.2 (2)
Se8–Mo1–Se9	52.7 (2)	Se5–Mo2–Se10	90.5 (2)	Mo3–Se6–Se7	62.2 (2)	Mo3–Se11–Se10	62.2 (2)
Se8–Mo1–Se13	83.3 (2)	Se5–Mo2–Se11	93.3 (2)	Mo3–Se7–Se6	63.9 (2)	Mo1–Se12–Mo3	63.6 (2)
Se9–Mo1–Se12	168.4 (3)	Se8–Mo2–Se9	52.8 (2)	Mo1–Se8–Mo2	65.2 (2)	Mo1–Se12–Se13	61.9 (2)
Se12–Mo1–Se13	53.1 (2)	Se8–Mo2–Se10	83.5 (2)	Mo1–Se8–Se9	64.2 (2)	Mo3–Se12–Se13	61.8 (2)
Se1–Mo1–Se3	92.5 (3)	Se9–Mo2–Se11	167.9 (3)	Mo2–Se8–Se9	65.2 (2)	Mo1–Se13–Mo3	65.7 (2)
Se1–Mo1–Se9	86.0 (2)	Se10–Mo2–Se11	53.4 (2)			Mo1–Se13–Se12	65.1 (3)
Se1–Mo1–Se12	83.1 (2)			Mo2–Mo1–Mo3	59.8 (1)	Se11–Se10–Se14	167.6 (4)
Se6–Mo3–Se10	90.1 (2)	Se7–Mo3–Se11	86.9 (2)	Mo1–Mo2–Mo3	60.1 (1)	Se8–Se9–Se14	167.5 (3)
Se6–Mo3–Se11	94.2 (2)	Se1–Mo3–Se11	84.0 (2)	Mo1–Mo3–Mo2	60.1 (1)	Se12–Se13–Se14	166.3 (4)
Se12–Mo3–Se13	53.1 (2)	Se1–Mo3–Se12	83.0 (3)				
Se6–Mo3–Se12	93.7 (2)	Se6–Mo3–Se7	53.9 (2)				
Se6–Mo3–Se13	90.4 (3)	Se10–Mo3–Se13	85.3 (2)				
Se1–Mo3–Se7	93.3 (3)	Se7–Mo3–Se12	88.3 (2)				
Se10–Mo3–Se11	53.4 (2)						
				Subcluster B			
Se14–Mo4–Se16	91.1 (2)	Se14–Mo6–Se24	83.4 (2)	Mo3–Se13–Se12	65.1 (2)	Mo4–Se22–Se21	61.7 (2)
Se14–Mo4–Se22	83.1 (2)	Se17–Mo5–Se24	88.3 (2)	Mo4–Se14–Mo5	68.7 (2)	Mo5–Se22–Se21	61.8 (2)
Se14–Mo4–Se26	83.4 (2)	Se18–Mo5–Se21	95.7 (2)	Mo4–Se14–Mo6	67.9 (2)	Mo5–Se23–Mo6	65.8 (2)
Se15–Mo4–Se16	53.2 (2)	Se18–Mo5–Se22	95.4 (2)	Mo5–Se14–Mo6	67.4 (2)	Mo5–Se23–Se24	63.2 (2)
Se15–Mo4–Se21	96.0 (2)	Se18–Mo5–Se23	93.2 (2)	Mo4–Se15–Se16	63.1 (2)	Mo4–Se25–Mo6	65.9 (2)
Se15–Mo4–Se22	97.2 (2)	Se21–Mo5–Se22	54.3 (2)	Mo4–Se16–Se15	63.7 (2)	Mo4–Se25–Se26	61.6 (2)
Se15–Mo4–Se25	92.4 (2)	Se21–Mo5–Se23	81.2 (2)	Mo5–Se17–Se18	64.1 (2)	Mo6–Se25–Se26	63.1 (2)
Se15–Mo4–Se26	90.9 (2)	Se22–Mo5–Se24	166.7 (2)	Mo5–Se18–Se17	61.8 (2)	Mo4–Se26–Mo6	65.0 (2)
Se16–Mo4–Se22	87.1 (2)	Se23–Mo5–Se24	55.0 (2)	Mo6–Se19–Se20	64.6 (3)	Mo4–Se26–Se25	61.7 (2)
Se16–Mo4–Se25	132.1 (2)	Se14–Mo5–Se17	89.6 (2)	Mo6–Se20–Se19	62.5 (3)	Mo6–Se26–Se25	60.5 (2)
Se16–Mo4–Se26	88.3 (2)	Se14–Mo5–Se22	82.8 (2)	Mo4–Se21–Mo5	66.1 (2)	Mo6–Se23–Se24	64.1 (2)
Se21–Mo4–Se22	54.5 (2)	Se14–Mo5–Se24	84.8 (2)	Mo4–Se21–Se22	64.0 (2)	Mo5–Se24–Mo6	64.4 (2)
Se21–Mo4–Se25	80.3 (2)	Se17–Mo5–Se18	54.2 (2)	Mo5–Se21–Se22	63.9 (2)	Mo5–Se24–Se23	61.9 (2)
Se22–Mo4–Se26	165.6 (3)	Se17–Mo5–Se22	86.9 (2)	Mo4–Se22–Mo5	64.6 (2)	Mo6–Se24–Se23	61.3 (2)
Se25–Mo4–Se26	56.8 (2)	Se14–Mo6–Se26	81.7 (2)	Se22–Se21–Se40	165.5 (3)	Mo5–Mo4–Mo6	59.7 (1)
Se23–Mo6–Se24	54.6 (2)	Se19–Mo6–Se20	52.9 (3)	Se26–Se25–Se40	165.3 (3)	Mo4–Mo5–Mo6	59.9 (1)
Se23–Mo6–Se25	81.0 (2)	Se19–Mo6–Se24	88.6 (2)	Se24–Se23–Se40	162.9 (3)	Mo4–Mo6–Mo5	60.4 (1)
Se23–Mo6–Se24	54.6 (2)	Se19–Mo6–Se26	87.6 (2)				
Se23–Mo6–Se25	81.0 (2)	Se20–Mo6–Se23	93.2 (3)				
Se24–Mo6–Se26	164.3 (3)	Se20–Mo6–Se24	95.1 (2)				
Se25–Mo6–Se26	56.5 (2)	Se20–Mo6–Se25	92.4 (3)				
Se14–Mo6–Se19	93.3 (3)	Se20–Mo6–Se26	94.8 (2)				
				Subcluster C			
Se27–Mo7–Se28	93.6 (2)	Se30–Mo8–Se31	53.9 (2)	Mo8–Se34–Se35	64.4 (2)	Mo7–Se27–Mo8	67.3 (2)
Se27–Mo7–Se35	83.1 (2)	Se30–Mo8–Se35	85.8 (2)	Mo7–Se35–Mo8	64.0 (2)	Mo7–Se27–Mo9	67.2 (2)
Se27–Mo7–Se39	84.0 (2)	Se30–Mo8–Se36	88.5 (2)	Mo7–Se35–Se34	61.3 (2)	Mo8–Se27–Mo9	66.5 (2)
Se31–Mo8–Se34	94.0 (2)	Se31–Mo8–Se36	92.0 (2)	Mo8–Se35–Se34	61.4 (2)	Mo7–Se28–Se29	65.1 (2)
Se28–Mo7–Se35	88.5 (2)	Se31–Mo8–Se37	91.2 (3)	Mo8–Se36–Mo9	63.9 (2)	Mo7–Se29–Se28	61.5 (2)
Se29–Mo7–Se39	95.1 (2)	Se34–Mo8–Se35	54.1 (2)	Mo8–Se36–Se37	60.9 (2)	Mo8–Se30–Se31	63.5 (2)
Se28–Mo7–Se29	53.4 (2)	Se34–Mo8–Se37	83.6 (2)	Mo9–Se36–Se37	61.0 (2)	Mo8–Se31–Se30	62.6 (2)
Se28–Mo7–Se39	88.5 (2)	Se35–Mo8–Se36	165.3 (3)	Mo8–Se37–Mo9	66.3 (2)	Mo9–Se32–Se33	64.4 (2)
Se29–Mo7–Se35	93.7 (2)	Se36–Mo8–Se37	54.7 (2)	Mo8–Se37–Se36	64.4 (2)	Mo9–Se33–Se32	61.9 (2)
Se34–Mo7–Se35	53.8 (2)	Se27–Mo8–Se30	91.3 (2)	Mo9–Se37–Se36	64.4 (2)	Mo7–Se34–Mo8	66.2 (2)
Se34–Mo7–Se38	81.7 (2)	Se27–Mo8–Se35	83.4 (2)	Mo7–Se38–Mo9	66.1 (2)	Mo7–Se34–Se35	64.9 (2)
Se35–Mo7–Se39	166.4 (3)	Se27–Mo8–Se36	83.2 (2)	Mo7–Se38–Se39	63.6 (2)		
Se38–Mo7–Se39	54.7 (2)	Se27–Mo8–Se37	113.2 (2)	Mo9–Se38–Se39	64.4 (2)	Se21–Se40–Se23	69.6 (2)
Se27–Mo9–Se32	94.4 (2)	Se37–Mo9–Se38	82.5 (3)	Mo7–Se39–Mo9	64.2 (2)	Se21–Se40–Se25	71.4 (2)
Se33–Mo9–Se36	93.1 (3)	Se32–Mo9–Se39	85.4 (2)	Mo7–Se39–Se38	61.7 (2)	Se23–Se40–Se25	70.0 (2)
Se27–Mo9–Se36	82.9 (2)	Se33–Mo9–Se37	89.8 (3)	Mo9–Se39–Se38	60.8 (2)	Se23–Se40–Se38	89.2 (2)
Se27–Mo9–Se37	112.7 (2)	Se33–Mo9–Se38	91.6 (3)	Se34–Se40–Se38	69.5 (2)	Se25–Se40–Se34	106.4 (3)
Se27–Mo9–Se38	113.1 (2)	Se33–Mo9–Se39	95.7 (3)	Mo8–Mo7–Mo9	59.4 (1)	Se35–Se34–Se40	167.1 (3)
Se27–Mo9–Se39	83.5 (2)	Se36–Mo9–Se37	54.6 (2)	Mo7–Mo8–Mo9	60.3 (1)	Se39–Se38–Se40	169.0 (3)
Se32–Mo9–Se33	53.7 (2)	Se36–Mo9–Se39	165.3 (3)	Mo7–Mo9–Mo8	60.2 (1)		
Se32–Mo9–Se36	90.2 (2)	Se38–Mo9–Se39	54.9 (2)				

[a] Numbers in parentheses are the estimated standard deviations in the least significant digits.

(2) to 3.182 (9) Å. An inverse correlation exists between the Se_{ap}–Se_a distance and the corresponding Se_a–Se_b distance. For example, the shortest Se_{ap}–Se_a distance, 2.80 (2) Å, results in the maximum lengthening of the corresponding diselenide to 2.44 (1) Å, which is 0.10 Å longer than the average bridging Se–Se distance in I and close to 2.45 (1) Å, the corresponding distance in $[Mo_{12}Se_{56}]^{12-}$.[12] Assuming that subclusters A and B in II are not bonded, the compound can be represented as $K_8[Mo_3Se_{13}]\cdot[Mo_6Se_{27}]\cdot 4H_2O$.

These results make it apparent that the pocket created by the three bridging Se_2^{2-} ligands of a trinuclear $[Mo_3Se_7]^{4+}$ core is special and that it has affinity for additional electron density, as

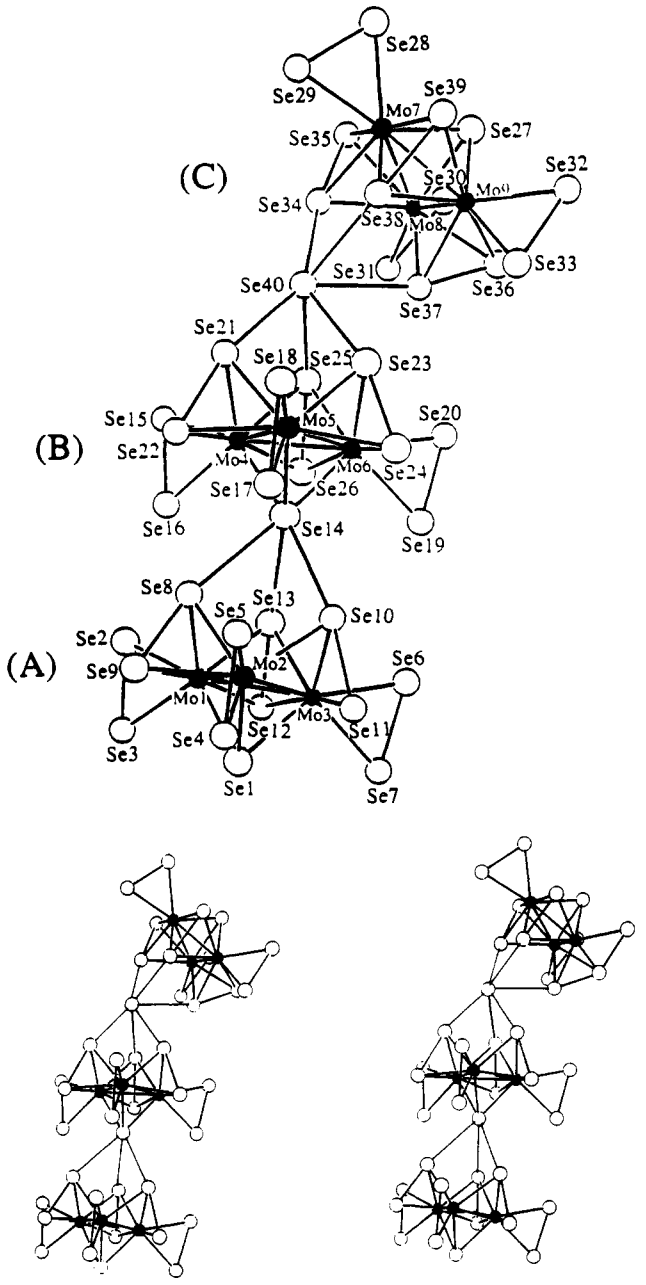

Figure 5. Top: ORTEP representation and labeling scheme of the $[Mo_9Se_{40}]^{8-}$ anion. Bottom: Stereoview of the $[Mo_9Se_{40}]^{8-}$ anion. Black circles represent Mo atoms.

if it was positively charged. The stabilization of such unusual polyselenide $[Se_x]^{n-}$ fragments with unconventional Se–Se distances appears to be a recurring theme in hydrothermal Mo/Se_x chemistry. It suggests that the lowest unoccupied molecular orbital on the $[Mo_3Se_7]^{4+}$ core is centered on the bridging diselenide ligands.

The reason for these long Se···Se interactions under such synthetic conditions is not clear at the moment, but it may be associated with the combination of higher temperature and pressure conditions and even the counterion used. We are currently investigating the counterion effect on these anions by looking at other cations besides K^+ to determine their role in directing the structure of the Mo/Se anion and any $[Se_x]^{n-}$ fragments.

Finally, there is an unusually short intercluster Se28···Se28 distance of 2.98 (1) Å between two different $[Mo_9Se_{40}]^{8-}$ clusters involving a terminal diselenide ligand in subcluster C. The two $[Mo_9Se_{40}]^{8-}$ clusters involved in this close Se···Se contact are related by a crystallographic center of symmetry, as shown in Figure 6. A similar distance was also observed in the electron-poor $[W(CO)_5Se_2]_2^{2+}$ dimer (Se–Se = 3.015 Å)[25] and $Se_4S_2N_2^{2+}$ cation

Table VIII. K–Se Distances (Å) in $K_8[Mo_9Se_{40}]\cdot 4H_2O$[a]

Se1–K3	3.59 (2)	Se17–K4	3.29 (1)	Se26–K7	3.76 (3)
Se2–K1	3.32 (1)	Se17–K5	3.39 (2)	Se26–K8	3.79 (3)
Se2–K2	3.23 (1)	Se17–K6′	3.27 (2)	Se26–K8′	3.33 (3)
Se3–K1	3.48 (2)	Se17–K7′	3.65 (2)	Se26–K8′	3.56 (3)
Se4–K2	3.30 (1)	Se18–K6	3.46 (2)	Se27–K2	3.37 (1)
Se4–K5′	3.51 (2)	Se18–K6′	3.10 (3)	Se28–K2	3.55 (1)
Se5–K2	3.44 (1)	Se18–K7′	3.73 (3)	Se28–K5′	3.46 (2)
Se5–K4	3.70 (2)	Se18–K7′	3.21 (2)	Se29–K2	3.25 (1)
Se5–K5	3.85 (2)	Se19–K7	3.41 (3)	Se29–K4	3.48 (1)
Se5–K5′	3.60 (2)	Se19–K8′	3.54 (3)	Se29–K5	3.27 (2)
Se7–K1	3.32 (1)	Se20–K8	3.68 (3)	Se29–K6′	3.71 (2)
Se7–K3	3.30 (2)	Se20–K8′	3.88 (3)	Se30–K1	3.30 (1)
Se8–K2	3.98 (1)	Se21–K6	3.87 (2)	Se30–K3	3.45 (1)
Se11–K2	3.82 (1)	Se21–K7′	3.79 (2)	Se31–K1	3.68 (1)
Se12–K1	3.49 (1)	Se21–K7′	3.86 (2)	Se31–K3	3.27 (1)
Se12–K3	3.72 (1)	Se22–K4	3.55 (1)	Se31–K8	3.65 (3)
Se15–K7	3.33 (3)	Se22–K6′	3.60 (2)	Se32–K3	3.20 (1)
Se15–K7′	3.64 (2)	Se24–K6	3.75 (2)	Se32–K5	3.75 (2)
Se16–K2	3.68 (1)	Se24–K7	3.72 (2)	Se32–K5′	3.36 (3)
Se16–K4	3.67 (1)	Se24–K7′	3.81 (2)	Se33–K3	3.56 (2)
Se33–K5	3.62 (3)	Se35–K5′	3.42 (2)	Se38–K7′	3.84 (3)
Se34–K6	3.69 (3)	Se35–K6′	3.83 (3)	Se39–K4	3.83 (1)
Se34–K6′	3.35 (2)	Se36–K1	3.71 (1)	Se40–K7′	3.81 (2)
Se36–K3	3.82 (1)	Se39–K5	3.59 (2)	Se38–K4	3.26 (1)
		Se40–K6	3.38 (2)	Se35–K5	3.74 (2)

Se1–K1	3.747 (7)	Se11–K2	3.921 (7)
Se2–K1	3.389 (6)	Se12–K2	3.420 (7)
Se4–K1	3.532 (7)	Se12–K2	3.668 (7)
Se6–K1	3.884 (6)	Se2–K2	3.300 (6)
Se10–K1	3.728 (6)	Se14–K2	3.379 (7)
Se14–K1	3.341 (6)	Se3–K2	3.740 (6)
Se15–K1	3.365 (6)	Se15–K2	3.241 (7)
Se16–K1	3.775 (6)	Se17–K2	3.444 (7)
Se18–K1	3.763 (7)		

[a] Standard deviations are given in parentheses.

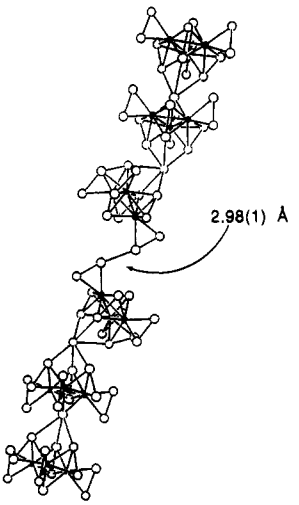

Figure 6. ORTEP representation of the centrosymmetric relationship between two clusters of $[Mo_9Se_{40}]^{8-}$. The short contact between two terminal diselenides is shown by the arrow. Black circles represent Mo atoms.

(Se–Se = 3.135 Å),[26] in which it was characterized as a weak Se···Se bonding interaction. These short Se···Se contacts are electronic in origin. The same cannot be said for the one encountered in II. If electron deficiency in the Mo(Se_2) fragment was causing this unusual Se···Se contact, shorter than average Mo–Se and Se–Se bonds would be expected. However, the normal Mo–Se and Se–Se distances, around the Mo–(Se_2) fragment, do not hint at any lack of electron density in this part of the molecule.

(25) Collins, M. J.; Gillespie, R. J.; Kolis, J. W.; Sawyer, J. F. *Inorg. Chem.* **1986**, *25*, 2057–2061.
(26) Gillespie, R. J.; Kent, J. P.; Sawyer, J. F. *Inorg. Chem.* **1981**, *20*, 4053–4060.

Thus, the close Se···Se distance may be the result of crystal packing forces.

Concluding Remarks

Thus far, all Mo/Se phases isolated contain recognizable $[Mo_3(\mu_2\text{-}Se_2)_3(\mu_3\text{-}Se)]^{4+}$ clusters connected by bridging selenide or polyselenide ligands. This extraordinarily stable $[Mo_3(\mu_2\text{-}Se_2)_3(\mu_3\text{-}Se)]^{4+}$ trinuclear core contains a triangular cavity created by the selenium atoms of the $\mu_2\text{-}Se_2^{2-}$ ligands which has the hitherto unrecognized property of attracting negatively charged species such as Se^{2-} or Se_x^{2-} ligands.

Hydrothermal synthesis with polychalcogenide ligands is a feasible and convenient technique to novel cluster or polymeric phases. Our work in this system alone points to an enormous wealth of new and different K/Mo/Se phases to be discovered. This synthesis is applicable to any cation/metal/chalcogenide system and thus has a very broad scope. We believe that future work in this new area of chalcogenide synthesis will lead to an abundance of novel structure types which may rival, in number, those of zeolites.

Acknowledgment. Financial support from the National Science Foundation for a Presidential Young Investigator Award is gratefully acknowledged. The X-ray instrumentation used in this work was purchased in part with funds from NSF Grant CHE-8908088. A generous gift from the EXXON Corp. is also acknowledged. M.G.K. is an A. P. Sloan Fellow (1991-1993). This work made use of the SEM facilities of the Center for Electron Optics, Michigan State University.

Supplementary Material Available: Tables of crystallographic data and structure refinement for $K_2Mo_3Se_{18}$ and $K_8Mo_9Se_{40}\cdot 4H_2O$, calculated and observed X-ray powder diffraction patterns, atomic coordinates of all atoms, and anisotropic and isotropic thermal parameters of all atoms for $K_2Mo_3Se_{18}$ and all non-hydrogen atoms for $K_8Mo_9Se_{40}\cdot 4H_2O$ (18 pages); listings of calculated and observed ($10F_o/10F_c$) structure factors (41 pages). Ordering information is given on any current masthead page.

Contribution from the Institute of Chemistry, Academia Sinica, Taipei, and Departments of Chemistry, National Taiwan Normal University, Taipei, and National Chung Hsing University, Taichung, Taiwan, Republic of China

Hydrothermal Synthesis and Structural Characterization of Two Calcium Vanadium(III) Phosphates: $Ca_2V(PO_4)(HPO_4)_2\cdot H_2O$ and $Ca_2V(PO_4)(P_2O_7)$

K. H. Lii,*,† N. S. Wen,‡ C. C. Su,‡ and B. R. Chueh§

Received August 15, 1991

The new phosphate $Ca_2V(PO_4)(HPO_4)_2\cdot H_2O$ and the dehydrated compound $Ca_2V(PO_4)(P_2O_7)$ have been synthesized hydrothermally at 230 and 450 °C, respectively, and characterized by single-crystal X-ray diffraction and thermogravimetric analysis. Crystal data: $Ca_2V(PO_4)(HPO_4)_2\cdot H_2O$, monoclinic, $C2/c$, a = 7.531 (2) Å, b = 15.522 (4) Å, c = 9.149 (2) Å, β = 113.52 (2)°, Z = 4, R = 0.0215 for 954 unique reflections; $Ca_2V(PO_4)(P_2O_7)$, monoclinic, $P2_1/c$, a = 6.391 (2) Å, b = 6.6362 (9) Å, c = 19.071 (2) Å, β = 99.26 (2)°, Z = 4, R = 0.029 for 1389 unique reflections. The structure of the hydrated compound consists of $^1_\infty[V(PO_4)_{2/2}(HPO_4)_{4/2}]$ along the [101] direction, which are held together by hydrogen bonding and O-Ca-O bonds. The structure of the dehydrated compound contains intersecting channels where the calcium atoms are located. The framework consists of corner-sharing VO_6 octahedra, PO_4 tetrahedra, and P_2O_7 groups. The connectivity formula is $^3_\infty Ca_2[V(PO_4)_{2/2}(P_2O_7)_{1/3}(P_2O_7)_{2/3}]$.

Introduction

We have recently found a number of new compounds in the alkali-metal vanadium phosphate system using high-temperature solid-state reactions. Compounds such as $Cs_2V_3P_4O_{17}$,[1] β-$K_2V_3P_4O_{17}$,[2] $A_2VOP_2O_7$ (A = Cs, Rb),[3] AVP_2O_7 (A = Li-Cs),[4-6] $NaVOPO_4$,[7] and $RbV_3P_4O_{17+x}$[8] were isolated. These phosphates often adopt tunnel or layer structures with the alkali-metal cations located in the tunnels or between the layers. Since the nature of the alkali-metal cations plays an important role in the crystal structures of these compounds, we have been interested in the synthesis and structural characterization of vanadium phosphates with divalent cations. Recently, we synthesized $Zn_2VO(PO_4)_2$ which contains a dimer of edge-sharing ZnO_5 square pyramids.[9] However, our efforts to grow crystals of vanadium phosphates containing alkaline-earth metals by the solid-state method have been unsuccessful, probably due to their very high melting points. Since the hydrothermal method is particularly suited for the synthesis of low-temperature phases and is also useful for the crystal growth, we have also been applying hydrothermal techniques to the synthesis of vanadium phosphates. Recent examples of vanadium phosphates from hydrothermal reactions include $K_2(VO)_2P_3O_9(OH)_3\cdot 1.125H_2O$,[10] $K_2(VO)_3(HPO_4)_4$,[11] β-$LiVOPO_4$,[12] $A_{0.5}VOPO_4\cdot xH_2O$ (A = Na, x = 2.0; A = K, x = 1.5),[13] and $Ni_{0.5}VOPO_4\cdot 1.5H_2O$.[14] We have extended our research aimed at synthesizing vanadium phosphates containing alkaline-earth metals by the hydrothermal method. At this time, we are able to grow crystals of calcium vanadium phosphates. To our knowledge, calcium vanadium phosphates are rare and up to now only the mineral sincosite, $Ca(VO)_2(PO_4)_2\cdot 5H_2O$, has been reported.[15] This paper describes the hydrothermal synthesis and structural characterization of $Ca_2V(PO_4)(HPO_4)_2\cdot H_2O$ and the dehydrated compound $Ca_2V(PO_4)(P_2O_7)$.

Experimental Section

Synthesis. $Ca(OH)_2$ (GR, Merck), $Ca_3(PO_4)_2$ (Merck), V_2O_3 (99.9%, Cerac), P_2O_5 (99.9%, Cerac), and H_3PO_4 (85%, Merck) were used as received. The conditions for the crystal growth of $Ca_2V(PO_4)(HPO_4)_2\cdot H_2O$ were as follows. A mixture of 1.0460 g of $Ca(OH)_2$ (14.12

† Academia Sinica.
‡ National Taiwan Normal University.
§ National Chung Hsing University.

(1) Lii, K. H.; Wang, Y. P.; Wang, S. L. *J. Solid State Chem.* **1989**, *80*, 127.
(2) Lii, K. H.; Tsai, H. J.; Wang, S. L. *J. Solid State Chem.* **1990**, *87*, 396.
(3) Lii, K. H.; Wang, S. L. *J. Solid State Chem.* **1989**, *82*, 239.
(4) Lii, K. H.; Wang, Y. P.; Chen, Y. B.; Wang, S. L. *J. Solid State Chem.* **1990**, *86*, 143.
(5) Wang, Y. P.; Lii, K. H.; Wang, S. L. *Acta Crystallogr.* **1989**, *C45*, 673.
(6) Wang, Y. P.; Lii, K. H. *Acta Crytallogr.* **1989**, *C45*, 1210.
(7) Lii, K. H.; Li, C. H.; Chen, T. M.; Wang, S. L. *Z. Kristallogr.* **1991**, *197*, 67.
(8) Lii, K. H.; Lee, C. S. *Inorg. Chem.* **1990**, *29*, 3298.
(9) Lii, K. H.; Tsai, H. J. *J. Solid State Chem.* **1991**, *90*, 291.
(10) Lii, K. H.; Tsai, H. J. *Inorg. Chem.* **1991**, *30*, 446.
(11) Lii, K. H.; Tsai, H. J. *J. Solid State Chem.* **1991**, *91*, 331.
(12) Lii, K. H.; Li, C. H.; Cheng, C. Y.; Wang, S. L. *J. Solid State Chem.*, in press.
(13) Wang, S. L.; Kang, H. Y.; Cheng, C. Y.; Lii, K. H. *Inorg. Chem.* **1991**, *30*, 3496.
(14) Lii, K. H.; Mao, L. F. *J. Solid State Chem.*, in press.
(15) Zolensky, M. E. *Am. Mineral.* **1985**, *70*, 409.

0020-1669/92/1331-0439$03.00/0